

Perturbation study on the spin and charge susceptibilities of the two-dimensional Hubbard model

Takashi Hotta

Institute for Solid State Physics, University of Tokyo, 7-22-1 Roppongi, Minato-ku, Tokyo 106, Japan

Satoshi Fujimoto

Department of Physics, Kyoto University, Kyoto 606, Japan

(October 8, 2018)

We investigate the spin and charge susceptibilities of the two-dimensional Hubbard model based upon the perturbative calculation in the strength of correlation U . For U comparable to a bare bandwidth, the charge susceptibility decreases near the half-filling as hole-doping approaches zero. This behavior suggesting the precursor of the Mott-Hubbard gap formation cannot be obtained without the vertex corrections beyond the random phase approximation. In the low-temperature region, the spin susceptibility deviates from the Curie-Weiss-like law and finally turns to decrease with the decrease of temperature. This spin-gap-like behavior is originating from the van Hove singularity in the density of states.

I. INTRODUCTION

The Hubbard model¹ has been studied extensively as the fundamental model for strongly correlated electron systems which exhibit the Mott-Hubbard metal-insulator transition (MIT)². Especially, the two-dimensional Hubbard model (2DHM) has been attracted much attention in relation to high-temperature superconductors (HTSC) of which normal metallic phase is quite “anomalous” in the sense that its property seriously deviates from that predicted by the conventional Fermi-liquid theory. Thus in this paper, we investigate 2DHM putting stress on the correlation effects on the charge and spin susceptibilities and grasp the signal of the “anomalous” behavior in the charge and spin responses near MIT from the weak-coupling perturbation approach.

As for the charge degree of freedom, we are interested in the dependence on hole-doping δ of the charge susceptibility. Since the system becomes incompressible near MIT, it is generally expected that the charge susceptibility decreases and eventually vanishes when we approach MIT by putting δ as zero. In fact, such a behavior has been obtained in some numerical studies on the basis of the quantum Monte Carlo (QMC) method.^{3,4} A quite different result, however, has been reported in QMC simulations⁵: The charge susceptibility diverges like $\sim 1/\delta$ as δ approaches zero. The difference between two results is not brought about by the scatter of the QMC data among the groups, but is originating from the physical interpretation of data. Thus it is desirable to investigate the doping dependence of the charge susceptibility with use of other methods. In this paper, by using the second-order perturbation theory (SOPT) with respect to the on-site Coulomb interaction U , we investigate the tendency of the change of the charge sus-

ceptibility from that in the non-interacting case due to correlation effects.

On the other hand, as for an anomalous behavior of the spin response, we would like to note the spin-gap-like behavior observed in the nuclear spin relaxation rate T_1^{-1} of several HTSC materials.⁶⁻¹⁴ In the higher-temperature region than the superconducting transition temperature T_c , $(T_1 T)^{-1}$ increases in proportional to $1/(T + \theta)$ with the decrease of T , indicating that $(T_1 T)^{-1}$ obeys the Curie-Weiss law. Here θ is the Weiss temperature. As T is decreased, in such materials as $\text{La}_{1-x}\text{Sr}_x\text{CuO}_4$ ⁶ and $\text{YBa}_2\text{Cu}_3\text{O}_{7-\delta}$ with $T_c \sim 90\text{K}$,^{7,8} $(T_1 T)^{-1}$ continues to increase until there occurs the transition to superconducting state. However, in such materials as $\text{YBa}_2\text{Cu}_3\text{O}_{6.6}$ with $T_c \sim 60\text{K}$,⁸⁻¹⁰ $\text{YBa}_2\text{Cu}_4\text{O}_8$,¹¹⁻¹³ and $\text{Bi}_2\text{Sr}_2\text{CaCuO}_8$,¹⁴ $(T_1 T)^{-1}$ begins to deviate from the Curie-Weiss law even for $T > T_c$, and turns to decrease with the decrease of T . Since this decrease of $(T_1 T)^{-1}$ seems to be associated with the formation of the spin-singlet state, such a behavior has been frequently called “the spin gap”. Some authors have argued the origin of the spin-gap formation such as the spinon pairing¹⁵ or bi-layer coupling,¹⁶ but it should be clarified whether it is possible or not to reproduce the spin-gap behavior in the framework of the Fermi-liquid theory without bi-layer coupling. From the analysis of the normal state of HTSC on the basis of the Fermi-liquid theory in due consideration of anti-ferromagnetic (AF) spin fluctuations,¹⁷ the following relation holds in HTSC:

$$(T_1 T)^{-1} \propto \chi_s(\mathbf{Q}, 0), \quad (1.1)$$

where $\chi_s(\mathbf{Q}, 0)$ is the staggered spin susceptibility in the static limit with $\mathbf{Q} = (\pi, \pi)$. Thus in this paper, by calculating $\chi_s(\mathbf{Q}, 0)$ in SOPT, we make a qualitative investigation on the temperature dependence of $(T_1 T)^{-1}$ of 2DHM.

By using the perturbative calculation, several authors have studied 2DHM so far,^{18–20} but the spin and charge susceptibilities which reflect the correlation effects on the spin and charge excitation have not been studied well even from the view point of SOPT. Although the perturbation method is not appropriate for the description of phase transition such as MIT, it is useful to study how correlation effects modify the behavior of these quantities in the Fermi-liquid phase and cause “anomalous” behaviors. We can point out such a merit of the perturbative approach that it is free from size effects compared with numerical simulations and suitable for the description of the low-energy properties. On the other hand, there exists such a demerit that the perturbative calculation will fail down for enough large value of U . However, as is seen in the perturbation study of the single impurity Anderson model, the expansion in terms of U is expected to converge asymptotically unless the spontaneous symmetry breaking occurs, leading to that the truncation of the expansion in second order may give a qualitatively correct description of some physical properties. Moreover, SOPT is helpful to grasp some features in the limit of large value of U . For example, it properly predicts the location of the Mott-Hubbard band at half-filling. In this sense, we may expect that our results on the spin and charge susceptibilities are qualitatively valid even for large value of U near half-filling. Thus it is meaningful to study the strong correlation effects within SOPT.

In order to evaluate the spin and charge susceptibilities properly in the vicinity of the half-filling, we take into account the vertex corrections which are not included in the random phase approximation (RPA). These corrections are considered to be important in two-dimensional systems, because the charge and spin fluctuations which destroy long-range order are large and a simple mean-field description such as RPA will not be valid. Actually, the vertex corrections beyond RPA are important for the description of the charge excitations near the half-filling as we will see later. The calculation is performed in the framework of the well-known Green’s function formalism. In order to carry out the complicated numerical computation, we exploit the Fast-Fourier-Transformation (FFT) algorithm.

The organization of this paper is as follows. In Sec. II, we develop the formulation to perform our calculation on the basis of the microscopic Fermi-liquid theory. In Sec. III, the numerical results for the charge susceptibility are given. We investigate the usual Hubbard model only with nearest-neighbor hopping terms as well as the model with next nearest-neighbor hopping ones which deforms the shape of the Fermi surface and changes the location of the van Hove singularity (VHS). For U comparable to the nearest-neighbor hopping energy, the charge susceptibility decreases as δ approaches zero due to the suppression effect of the vertex corrections. In Sec. IV, we show our numerical results for the dependence on δ as well as T of the spin susceptibility. In the low-temperature region, the spin susceptibility shows spin-gap-like behavior due

to VHS in the density of states (DOS). Finally in Sec. V, we summarize this paper and briefly comment on the relation between our results and NMR experimental results in HTSC. We will employ units in which both \hbar and k_B are taken to unity.

II. FORMULATION

A. Model Hamiltonian

Let us consider tight-binding electrons on the two-dimensional square lattice. The non-interacting part of the Hamiltonian consists of the hopping term between nearest- and next nearest-neighbor sites. We take into account the on-site Coulomb repulsion U . Thus, we obtain the following model Hamiltonian:

$$H = \sum_{\mathbf{k}\sigma} (E_{\mathbf{k}} - \mu) c_{\mathbf{k}\sigma}^\dagger c_{\mathbf{k}\sigma} + (U/N) \sum_{\mathbf{k}, \mathbf{k}', \mathbf{q} (\neq 0)} c_{\mathbf{k}-\mathbf{q}\uparrow}^\dagger c_{\mathbf{k}'+\mathbf{q}\downarrow}^\dagger c_{\mathbf{k}'\downarrow} c_{\mathbf{k}\uparrow}, \quad (2.1)$$

where $c_{\mathbf{k}\sigma}$ is the annihilation operator of an electron with momentum \mathbf{k} and spin σ , μ the chemical potential, U the on-site Coulomb interaction and N the number of sites. The electronic dispersion relation is given by

$$E_{\mathbf{k}} = -t(\cos k_x + \cos k_y) - t' \cos k_x \cos k_y, \quad (2.2)$$

where t and t' are, respectively, proportional to nearest and next-nearest neighbor hopping integrals.

B. Self-energy in SOPT

In general, the one-electron Green’s function $G(k)$ is expressed as

$$G(k) = \frac{1}{i\epsilon_n + \mu - E_{\mathbf{k}} - \Sigma(k)}, \quad (2.3)$$

where $\Sigma(k)$ is the electronic self-energy, k denotes $(\mathbf{k}, i\epsilon_n)$, $\epsilon_n \equiv \pi T(2n+1)$ with an integer n is the fermion Matsubara frequency at a temperature T , and μ is determined through the relation

$$n = 2 \sum_k G(k) e^{i\epsilon_n \eta}. \quad (2.4)$$

Here n is the number density of electron, η is the positive infinitesimal, and we use such a shorthand notation as

$$\sum_k \equiv T \sum_n \sum_{\mathbf{k}}. \quad (2.5)$$

With use of n , the hole-doping δ is defined as

$$\delta \equiv 1 - n. \quad (2.6)$$

The Hartree term of the self-energy is expressed as

$$\Sigma_H = U \sum_k G(k) e^{i\epsilon_n \eta}, \quad (2.7)$$

which is equal to $Un/2$, leading to a constant energy shift. Thus, we define the Green's function in the Hartree approximation, $G_0(k)$, as

$$G_0(k) = \frac{1}{i\epsilon_n + \mu_0 - E_k}, \quad (2.8)$$

where μ_0 is determined through the relation Eq. (2.4) in which G is replaced with G_0 . In this number-conserving approximation, the Hartree term is automatically taken into account in G_0 . Therefore in the following, we do not include the Hartree term explicitly in each order term.

Since the Hartree term is absorbed into μ_0 , we need to calculate only the second-order term of the self-energy, given by

$$\Sigma(k) = U^2 \sum_{k'} \chi_0(k - k') G_0(k'), \quad (2.9)$$

where $\chi_0(q)$ is defined by

$$\chi_0(q) = - \sum_k G_0(k) G_0(k + q). \quad (2.10)$$

Here we use another shorthand notation as $q = (\mathbf{q}, i\omega_\nu)$, where $\omega_\nu \equiv 2\pi T\nu$ with an integer ν is the boson Matsubara frequency.

Let us evaluate μ within SOPT, expressed as

$$\mu = \mu_0 + \delta\mu, \quad (2.11)$$

where $\delta\mu$ is the chemical potential due to the second-order term. From Eqs. (2.3), (2.8), (2.9), and (2.11), up to second order in U , n in Eq. (2.4) is expressed as

$$n = 2 \sum_k G_0(k) e^{i\epsilon_n \eta} + 2 \sum_k G_0^2(k) [\Sigma(k) - \delta\mu]. \quad (2.12)$$

Since the electron number is conserved, $\delta\mu$ is given by

$$\delta\mu = - \frac{1}{\chi_0(0)} \sum_k G_0^2(k) \Sigma(k). \quad (2.13)$$

In the following, we rewrite $\Sigma(k) - \delta\mu$ as $\Sigma(k)$.

C. Charge and spin susceptibilities in SOPT

We define $\chi_s(q)$ and $\chi_c(q)$ as

$$\chi_c(q) = \int_0^{1/T} d\tau e^{i\omega_\nu \tau} \langle T_\tau [\Delta n_{\mathbf{q}}(\tau) \Delta n_{-\mathbf{q}}] \rangle, \quad (2.14)$$

and

$$\chi_s(q) = (g\mu_B)^2 \int_0^{1/T} d\tau e^{i\omega_\nu \tau} \langle T_\tau [S_{\mathbf{q}}^z(\tau) S_{-\mathbf{q}}^z] \rangle, \quad (2.15)$$

where $S_{\mathbf{q}}^z$ and $\Delta n_{\mathbf{q}}$ are, respectively, given by

$$S_{\mathbf{q}}^z = (1/2) \sum_{\mathbf{k}} [c_{\mathbf{k}+\mathbf{q}\uparrow}^\dagger c_{\mathbf{k}\uparrow} - c_{\mathbf{k}+\mathbf{q}\downarrow}^\dagger c_{\mathbf{k}\downarrow}], \quad (2.16)$$

and $\Delta n_{\mathbf{q}} = n_{\mathbf{q}} - \langle n_{\mathbf{q}} \rangle$ with

$$n_{\mathbf{q}} = \sum_{\mathbf{k}\sigma} c_{\mathbf{k}+\mathbf{q}\sigma}^\dagger c_{\mathbf{k}\sigma}. \quad (2.17)$$

Here g is the electron g -factor and μ_B is the Bohr magneton. The magnetic unit is fixed as $g\mu_B/2 = 1$.

Equations (2.14) and (2.15) can be recast into

$$\chi_c(q) = 2[\chi^{\uparrow\uparrow}(q) + \chi^{\uparrow\downarrow}(q)], \quad (2.18)$$

and

$$\chi_s(q) = 2[\chi^{\uparrow\uparrow}(q) - \chi^{\uparrow\downarrow}(q)], \quad (2.19)$$

respectively, where $\chi^{\sigma\sigma'}(q)$ is defined as

$$\chi^{\sigma\sigma'}(q) = \int_0^{1/T} d\tau e^{i\omega_\nu \tau} \langle T_\tau \sum_{\mathbf{k}} c_{\mathbf{k}+\mathbf{q}\sigma}^\dagger(\tau) c_{\mathbf{k}\sigma}(\tau) \times \sum_{\mathbf{p}} c_{\mathbf{p}+\mathbf{q}\sigma}^\dagger c_{\mathbf{p}\sigma} \rangle_{\text{conn}}, \quad (2.20)$$

where the subscript “conn” denotes the operation to take into account only connected diagrams. Expanding the right-hand side of Eq. (2.20) with respect to U up to second order in the framework of the conventional perturbation theory, we obtain $\chi^{\sigma\sigma'}(q)$ diagrammatically shown in Fig. 1. Combining Eqs. (2.18) and (2.19) with the explicit expressions for $\chi^{\sigma\sigma'}(q)$, we obtain $\chi_s(q)$ and $\chi_c(q)$ as

$$\chi_c(q) = 2[\chi_0(q) - U\chi_0^2(q) + U^2\chi_0^3(q) - \delta\chi(q) - U^2\{2\chi_{\text{corr1}}(q) + \chi_{\text{corr2}}(q)\}], \quad (2.21)$$

and

$$\chi_s(q) = 2[\chi_0(q) + U\chi_0^2(q) + U^2\chi_0^3(q) - \delta\chi(q) + U^2\chi_{\text{corr2}}(q)], \quad (2.22)$$

where both $\chi_{\text{corr1}}(q)$ and $\chi_{\text{corr2}}(q)$ indicate the vertex corrections which are not included in RPA and $\delta\chi(q)$ is the correction term due to the insertion of the self-energy. The expressions for $\chi_{\text{corr1}}(q)$, $\chi_{\text{corr2}}(q)$, and $\delta\chi(q)$ are given in the following:

$$\chi_{\text{corr1}}(q) = \sum_{k_1, k_2} G_0(k_1) G_0(k_1 + q) \chi_0(k_1 - k_2) \times G_0(k_2) G_0(k_2 + q), \quad (2.23)$$

$$\begin{aligned}\chi_{\text{corr}2}(q) &= \sum_{k_1, k_2} G_0(k_1) G_0(k_1 + q) \phi_0(k_1 + k_2) \\ &\times G_0(k_2) G_0(k_2 - q),\end{aligned}\quad (2.24)$$

with $\phi_0(q)$ defined by

$$\phi_0(q) \equiv - \sum_k G_0(k) G_0(q - k), \quad (2.25)$$

and

$$\delta\chi(q) = \sum_k G_0^2(k) \Sigma(k) [G_0(k + q) + G_0(k - q)]. \quad (2.26)$$

For the comparison, we also consider the susceptibilities calculated in RPA-like approximation up to second order in U , which are given by

$$\chi_c^{\text{RPA}}(q) = 2[\chi_0(q) - U\chi_0^2(q) + U^2\chi_0^3(q)], \quad (2.27)$$

and

$$\chi_s^{\text{RPA}}(q) = 2[\chi_0(q) + U\chi_0^2(q) + U^2\chi_0^3(q)]. \quad (2.28)$$

In the following, we call this approximation “second-order RPA (SO-RPA)”.

D. Method for numerical calculation

When we carry out sum over the momentum as well as the Matsubara frequency in the numerical calculation, the first Brillouin zone (FBZ) is divided into fine meshes and the frequency sum is terminated at a cut-off energy ω_c . In this paper, we perform the calculation on a 64×64 lattice from the limitation of computer memory. We should note an existence of a lower limit of temperature in which reliable results are obtained: As has been pointed out by Serene and Hess²², with a 64×64 lattice, the deviation from the Fermi-liquid behavior becomes significant at $T/t = 0.0075$ for our definition of t . Thus, our calculation will be carried out only for T larger than 0.01t.

As for the frequency cut-off, we always choose ω_c as $64t$, irrespective of T . Note that ω_c is equal to $16W$, where W is a bare bandwidth given by $4t$. Such a large value for the cut-off energy is considered to be sufficient to converge the frequency sum.²²

We briefly explain a means to perform the complicated sum over k efficiently. The point is to arrange the sum into the convolution form convenient for the FFT algorithm.^{21,22} For example, $\chi_{\text{corr}1}$ in Eq. (2.23) is rewritten as

$$\chi_{\text{corr}1}(q) = \sum_{k_1, k_2} C_1(k_1; q) \chi_0(k_1 - k_2) C_1(k_2; q), \quad (2.29)$$

where $C_1(k; q) = G_0(k) G_0(k + q)$. When we symbolically represent the Fourier transform of $\chi_0(q)$ and $C_1(k; q)$ as

$$\chi_0(q) = \sum_x e^{iqx} \chi_0(x), \quad (2.30)$$

and

$$C_1(k; q) = \sum_y e^{iky} C_1(y; q), \quad (2.31)$$

respectively, $\chi_{\text{corr}1}$ is expressed as

$$\chi_{\text{corr}1}(q) \propto \sum_x C_1(x; q) \chi_0(x) C_1(-x; q), \quad (2.32)$$

except for the normalization. Let us estimate the numerical steps necessary for the calculation with and without FFT. Assume that we need M steps to carry out sum over k . When we calculate $\chi_{\text{corr}1}$ in Eq. (2.23) without FFT for a fixed q , the steps of the order of M^2 are necessary. On the other hand, if we exploit the FFT algorithm for the calculation of $\chi_{\text{corr}1}$ in Eq. (2.32), we need only the steps of the order of $M \log_2 M$ to finish all the sums. This difference leads us a drastic reduction of the task in the numerical calculation.

III. CALCULATED RESULTS FOR CHARGE SUSCEPTIBILITY

A. Doping dependence

Now we investigate the dependence on δ of the uniform charge susceptibility in the static limit, χ_c . We first consider the case only with nearest-neighbor hopping in the dispersion relation given by Eq. (2.2). The results for this case are shown in Fig. 2. For $U = 0$, χ_c increases logarithmically due to VHS, as δ approaches zero. In the interacting case, χ_c is totally suppressed both in SO-RPA and SOPT. For U comparable to t , χ_c still increases with the decrease of δ in SO-RPA, but in contrast, it turns to decrease near the half-filling in SOPT as δ approaches zero. The large suppression of χ_c in SOPT near the half-filling is due to the vertex corrections which are not included in RPA.

In order to discuss the physical meaning of our calculated results, we would like to comment on the relation between the formula for χ_c of the Landau’s Fermi-liquid theory and one of the microscopic Fermi-liquid theory developed by Luttinger.²³ In the Landau’s Fermi-liquid theory, χ_c is phenomenologically expressed as

$$\chi_c = \frac{m^*}{m} \frac{\chi_c^0}{1 + F_0^s}, \quad (3.1)$$

where m^* is the renormalized mass, χ_c^0 the bare susceptibility, and F_0^s the Landau’s parameter. Based upon the Luttinger’s formulation, we obtain another expression for χ_c as

$$\chi_c = \sum_{\mathbf{k}} \delta(E_{\mathbf{k}}^*) z_{\mathbf{k}} \left[1 - \frac{\partial \text{Re}\Sigma(\mathbf{k}, 0)}{\partial \mu} \right], \quad (3.2)$$

where $E_{\mathbf{k}}^*$ is the dispersion relation for the quasi-particle given by

$$E_{\mathbf{k}}^* = z_{\mathbf{k}} [E_{\mathbf{k}} - \mu + \text{Re}\Sigma(\mathbf{k}, 0)], \quad (3.3)$$

and $z_{\mathbf{k}}$ is the renormalization factor determined by

$$z_{\mathbf{k}}^{-1} = 1 - \frac{\partial \text{Re}\Sigma(\mathbf{k}, \omega)}{\partial \omega} \Big|_{\omega=0}. \quad (3.4)$$

Comparing Eq. (3.2) with Eq. (3.1), we notice approximately the following correspondence:

$$\frac{m^*}{m} \chi_s^0 \leftrightarrow \sum_{\mathbf{k}} \delta(E_{\mathbf{k}}^*), \quad (3.5)$$

and

$$\frac{1}{1 + F_0^s} \leftrightarrow z_{\mathbf{k}} \left[1 - \frac{\partial \text{Re}\Sigma(\mathbf{k}, 0)}{\partial \mu} \right]. \quad (3.6)$$

From Eq. (3.2), we see that χ_c is nothing but the average over the Fermi surface of the factor $1 - \partial \text{Re}\Sigma / \partial \mu$. It does not depend explicitly on the renormalized mass in contrast to Eq. (3.1), but is determined by the bare DOS and the factor $1 - \partial \text{Re}\Sigma / \partial \mu$ which is incorporated into our calculation as the vertex corrections. Thus the correlation effect on χ_c is essentially due to the factor $1 - \partial \text{Re}\Sigma / \partial \mu$. Note that χ_c is not enhanced by the renormalized mass m^* as naively expected from Eq. (3.1). This is contrasted with the one-dimensional Luttinger liquid where the charge susceptibility is determined solely by the renormalized DOS.²⁴

Our numerical results imply that $1 - \partial \text{Re}\Sigma / \partial \mu$ tends to be zero as μ approaches the half-filling value, suggesting that χ_c vanishes continuously if we can describe the MIT transition properly. Our results are consistent with that of the QMC simulations by Moreo *et. al.*³ and Otsuka⁴ but not with the assertion by Furukawa and Imada⁵ that the charge susceptibility diverges in the vicinity of the half-filling. In the framework of the Fermi-liquid theory, the increase of the charge susceptibility due to correlation effects does not occur as discussed above. Thus the conclusion in Ref. 5 implies that some non-Fermi-liquid state realizes in the metallic phase near MIT. However, the results in the infinite-dimensional Hubbard model indicate that there is no intermediate exotic state between the Fermi-liquid metallic phase and the Mott insulating phase.²⁵ Since no symmetry breaking occurs at finite temperature in two-dimensional systems, we expect that there is no phase transition from the Fermi-liquid state to a non-Fermi-liquid one as n approaches unity. Thus our results based upon the Fermi-liquid theory plausibly may describe the qualitative behavior of the charge susceptibility near MIT.

B. Effects of next-nearest neighbor hopping

Since χ_c depends on the bare DOS, it is sensitively affected by the band structure. In this subsection, we consider the effect of the next-nearest hopping term which changes the location of VHS and deforms the shape of the Fermi surface. The results for the case of $t'/t = 0.2$ is shown in Fig. 3. It can be seen that χ_c increases monotonically as δ approaches zero, indicating that we cannot obtain the suppression effect large enough to overcome the enhancement of the bare DOS due to VHS. In this case, VHS is located in the region of $\omega > 0$, where ω is the energy measured from the Fermi level. Thus the bare DOS at the Fermi level is always too small to produce strong correlation effects through the vertex corrections when we decrease hole-doping by changing the chemical potential. The suppression effect due to the vertex corrections is weak when the bare DOS at the Fermi level is not large enough. This tendency can be confirmed from the results for the case of $t'/t = -0.2$, which are shown in Fig. 4. In this case, VHS is located in the region of $\omega < 0$. When δ is decreased with the change of μ , the Fermi level inevitably crosses the position of VHS at some value of μ . At the corresponding hole doping, χ_c shows a shallow minimum for $U/t = 1.0$. This minimum is due to the maximum of the suppression effect of the vertex corrections. Thus we conclude that the large bare DOS at the Fermi level results in the strong suppression effect of χ_c through the vertex corrections which overcomes the enhancement effect of χ_c due to the bare DOS, leading to the total decrease of χ_c in the vicinity of MIT.

IV. CALCULATED RESULTS FOR SPIN SUSCEPTIBILITY

A. Doping Dependence

Let us discuss the numerical results for the static spin susceptibility at $\mathbf{q} = \mathbf{Q}$, χ_s . The dependence on δ of χ_s is depicted in Fig. 5. Because of the nesting properties of the Fermi surface, the AF correlation develops near the half-filling and results in the enhancement of χ_s . We also show the results for the case in the presence of the next nearest-neighbor hopping t' in Figs. 6 and 7. In both cases of $t' = 0.2$ and $t' = -0.2$, the nesting properties of the Fermi surface is much weakened. Thus the enhancement of AF correlation is reduced compared with the case for $t' = 0$, but there is no qualitative difference in the doping dependence between these cases.

B. Temperature Dependence: Spin-gap-like Behavior

In this subsection, we investigate the temperature dependence of χ_s . The results for the case with only the nearest-neighbor hopping are shown in Fig. 8. The electron number is chosen as $n = 0.94$. In the high-temperature region, χ_s follows the Curie-Weiss-like behavior. On the other hand, in the low-temperature region, the spin-gap-like behavior manifests. Since it is observed even in the case of $U = 0$, this spin-gap-like behavior is essentially due to the band effect: In the non-half-filled case, VHS's at $\mathbf{k} = (\pm\pi, \pm\pi)$ are not on the Fermi surface and then the contributions from VHS to the spin susceptibility decrease as the temperature is lowered. Consequently, χ_s shows the spin-gap-like behavior in the low-temperature region. Although the spin-gap-like behavior is very small for $U = 0$ near the half-filling, it is much enhanced due to the correlation effect and results in the large spin-gap-like behavior as shown in Fig. 8. Note that such enhancement is not brought about by the speciality of RPA, because we also obtain the robust spin-gap-like structure even with the vertex corrections beyond RPA.

When we introduce the next nearest-neighbor hopping, the spin-gap-like behavior disappears as shown in Figs. 9 and 10 for $t' = 0.2$ and $t' = -0.2$, respectively, with $n = 0.94$. The next nearest-neighbor hopping changes band structure and the effect of VHS becomes too small to give rise the spin-gap behavior in these cases. For the case of $t' = -0.2$, the large enhancement in the low-temperature region can be understood as the effect of VHS, because the location of VHS is very close to the Fermi surface. At the lower temperature than $0.01t$, it is expected that the spin-gap behavior may manifest, but we do not carry out the calculation in this temperature region because of the lack of the reliability of our calculation on a 64×64 lattice as well as the limitation of computer memory. Instead of calculating χ_s at lower temperature, we obtain the temperature dependence of χ_s at $n = 0.86$. The results are shown in Fig. 11. Since the difference between the position of VHS and that of the Fermi level is $0.05t$ at this filling, the spin-gap-like behavior is observed even in the present temperature range in contrast to the case of $n = 0.94$. Thus our spin-gap behavior is originating from VHS, not the nesting property of the Fermi surface.

V. SUMMARY AND DISCUSSION

We have investigated the doping and temperature dependence of the charge and spin susceptibilities by using SOPT. The charge susceptibility is much suppressed due to the correlation effect through the vertex corrections in the vicinity of the half-filling for U comparable to t . It has been explicitly shown that the vertex corrections beyond RPA are indispensable in order to obtain this be-

havior. The suppression of the charge susceptibility near the half-filling indicates a precursor of the formation of the Mott-Hubbard gap. Such a behavior of the charge susceptibility will be qualitatively correct as long as the system is kept in the Fermi-liquid state, but we cannot perfectly deny the possibility that the charge susceptibility jumps abruptly from a finite value to zero or diverges at the half-filling if the system turns to be in a non-Fermi-liquid state due to the speciality of two-dimensional systems in combination with the strong correlation effect. In this sense, we need further studies beyond perturbative calculation in order to understand the behavior of the charge susceptibility near MIT in the two-dimensional Hubbard model.

In the study of the spin susceptibility, we have obtained the spin-gap-like behavior not only the case for $t' = 0$ but also the case with non-zero next nearest-neighbor hopping. The origin of our spin-gap-like behavior is ascribed to the band effect such as VHS in combination with the enhancement effect due to electron correlation: In the static spin susceptibility at $\mathbf{q} = (\pi, \pi)$, VHS gives rise to a small spin-gap-like structure, which will be much enhanced by correlation effects. We have emphasized that such an enhancement is not brought about by the speciality of RPA. Even if we take into account the diagrams for the vertex corrections beyond RPA, the same structure has been obtained. Those vertex corrections are important in the two-dimensional model in which quantum and thermal fluctuations destroy any long range order.

Finally, we give a brief comment on the spin gap in NMR experiments on HTSC.⁶⁻¹⁴ It has been argued that the origin of the spin-gap-like behavior observed in those experiments is the condensation of paired spinons in the RVB picture¹⁵ or the bi-layer coupling in the Fermi-liquid picture.¹⁶ As we have seen in this paper, even in the Fermi-liquid theory without bi-layer coupling, the spin-gap-like behavior has been reproduced by the effect of VHS combined with the enhancement effect due to electron correlation. Although it is difficult to adjust quantitatively the size of the gap and the band structure in our calculation to the experimental results, there are some indirect evidences which imply the relevance of VHS to the spin-gap behavior. In the NMR experimental result on $\text{YB}_2\text{Cu}_3\text{O}_{7-\delta}$ ¹⁰, it can be seen that the spin-gap behavior becomes weak as δ approaches zero. It has been pointed out that the DOS of $\text{YB}_2\text{Cu}_3\text{O}_{7-\delta}$ has a peak near the Fermi level due to VHS for $\delta = 0$ and this peak runs away from the Fermi level as δ increases²⁶. Thus it may be plausible to attribute the spin-gap-like behavior of this material to VHS in DOS enhanced due to strong electron correlation.

ACKNOWLEDGMENTS

The authors are grateful to K. Yamada, Y. Takada, N. Kawakami, M. Imada, H. Fukuyama, and N. Fu-

rukawa for useful conversations. This work has been supported by a Grant-in-Aid for Scientific Research on Priority Area “Anomalous Metallic State near the Mott Transition” (07237102) from the Ministry of Education, Science, Sports, and Culture, Japan.

¹ J. Hubbard, Proc. R. Soc. London **A281**, 401 (1964).
² N. F. Mott, Philos. Mag. **6**, 287 (1961).
³ A. Moreo, D. J. Scalapino, R. L. Sugar, S. R. White, and N. E. Bickers, Phys. Rev. **B41**, 2313 (1990).
⁴ H. Otsuka, J. Phys. Soc. Jpn. **59**, 2916 (1990).
⁵ N. Furukawa and M. Imada, J. Phys. Soc. Jpn. **60**, 3604 (1991).
⁶ Y. Kitaoka, S. Ohsugi, K. Ishida, and Y. Asayama, Physica C **170**, 189 (1990); S. Ohsugi, Y. Kitaoka, K. Ishida, and Y. Asayama, J. Phys. Soc. Jpn. **60**, 2351 (1991).
⁷ Y. Kitaoka, K. Ishida, S. Ohsugi, K. Fujiwara, and Y. Asayama, Physica C **185-189**, 98 (1991).
⁸ H. Yasuoka, T. Imai, and T. Shimizu, *Strong Correlation and Superconductivity*, (Springer-Verlag, Berlin, 1989), p. 254.
⁹ W. W. Warren, Jr., R. E. Walstedt, G. F. Brennert, R. J. Cava, R. Tycko, R. F. Bell, and G. Dabbagh, Phys. Rev. Lett. **62**, 1193 (1989).
¹⁰ M. Takigawa, A. P. Reyes, P. C. Hammel, J. D. Thompson, R. H. Heffner, Z. Fisk, and K. C. Ott, Phys. Rev. **B43**, 247

(1991).
¹¹ H. Zimmerman, M. Mali, D. Brinkman, J. Kapinsky, E. Kaldis, and S. Ruciecki, Physica C **159**, 681 (1989).
¹² T. Machi, I. Tomono, T. Miyataka, N. Koshizuka, S. Tanaka, T. Imai, and H. Yasuoka, Physica C **173**, 32 (1990).
¹³ G.-q. Zheng, T. Odaguchi, T. Mito, Y. Kitaoka, K. Asayama, and Y. Kodama, J. Phys. Soc. Jpn. **62**, 2591 (1993).
¹⁴ R. E. Walstedt, R. F. Bell, and D. B. Mitzi, Phys. Rev. B **44**, 7760 (1991).
¹⁵ T. Tanamoto, H. Kohno, and H. Fukuyama, J. Phys. Soc. Jpn. **61**, 1886 (1992); **62**, 717 (1993).
¹⁶ A. J. Millis and H. Monien, Phys. Rev. Lett. **70**, 2810 (1993).
¹⁷ H. Kohno and K. Yamada, Prog. Theor. Phys. **85**, 13 (1991).
¹⁸ H. Schweitzer and G. Czycholl, Z. Phys. **B83**, 93 (1991).
¹⁹ T. Hotta, J. Phys. Soc. Jpn. **64**, 2923 (1995).
²⁰ V. Zlatić, K. D. Schotte, and G. Schliecker, Phys. Rev. **B52**, 3639 (1995).
²¹ W. H. Press, B. P. Flannery, S. A. Tenkolsky and W. T. Vetterling : *Numerical Recipes*, (Press Syndicate of the University of Cambridge, New York, 1986), p.490.
²² J. W. Serene and D. W. Hess, Phys. Rev. **B44**, 3391 (1991).
²³ J. M. Luttinger, Phys. Rev. **119**, 1153 (1960).
²⁴ T. Usuki, N. Kawakami, and A. Okiji, Phys. Lett. **135A**, 476 (1989).
²⁵ M. J. Rosenberg, X. Y. Zhang, and G. Kotliar, Phys. Rev. Lett. **69**, 1236 (1992).
²⁶ C. C. Tsuei, C. C. Chi, D. M. Newns, P. C. Pattnaik, and M. Däumling, Phys. Rev. Lett. **69**, 2134 (1992).

FIG. 1. Diagrams for $\chi^{\sigma\sigma'}$ within second order with respect to the on-site Coulomb interaction U . The solid and the dashed lines, respectively, indicate the bare Green's function G_0 and U . Note that the Hartree term is included in the G_0 -line.

FIG. 2. Charge susceptibility plotted as a function of the hole-doping δ for $t' = 0$ and $T = 0.04t$. Open squares linked by thin solid line indicates the results for $U = 0$. The results for SO-RPA and SOPT for $U = t$ are denoted by open circles connected by broken line and solid circles linked by thick line, respectively.

FIG. 3. Charge susceptibility plotted as a function of the hole-doping δ for $t' = 0.2t$ and $T = 0.04t$. The results are shown in the same lines and symbols as in Fig. 2.

FIG. 4. Charge susceptibility plotted as a function of the hole-doping δ for $t' = -0.2t$ and $T = 0.04t$. The results are shown in the same lines and symbols as in Fig. 2.

FIG. 5. Spin susceptibility as a function of the hole-doping δ for $t' = 0$ and $T = 0.04t$. Open squares linked by this solid line indicates the results for $U = 0$. The results for SO-RPA and SOPT for $U = 0.5t$ are denoted by open circles connected by broken line and solid circles linked by thick line, respectively.

FIG. 6. Spin susceptibility as a function of the hole-doping δ for $t' = 0.2t$ and $T = 0.04t$. The results are shown in the same lines and symbols as in Fig. 5.

FIG. 7. Spin susceptibility as a function of the hole-doping δ for $t' = -0.2t$ and $T = 0.04t$. The results are shown in the same lines and symbols as in Fig. 5.

FIG. 8. Spin susceptibility plotted as a function of the temperature T for $t' = 0$ and $n = 0.94$. Open squares linked by this solid line indicates the results for $U = 0$. The results for SO-RPA and SOPT for $U = 0.5t$ are denoted by open circles connected by broken line and solid circles linked by thick line, respectively.

FIG. 9. Spin susceptibility plotted as a function of the temperature T for $t' = 0.2t$ and $n = 0.94$. The results are shown in the same lines and symbols as in Fig. 8.

FIG. 10. Spin susceptibility plotted as a function of the temperature T for $t' = -0.2t$ and $n = 0.94$. The results are shown in the same lines and symbols as in Fig. 8.

FIG. 11. Spin susceptibility plotted as a function of the temperature T for $t' = -0.2t$ and $n = 0.86$. The results are shown in the same lines and symbols as in Fig. 8.

$$\chi^M = \chi^{\downarrow\uparrow}$$

$$=$$

$$+$$

$$+$$

$$\chi^N = \chi^{\downarrow\uparrow}$$

$$=$$

$$+$$

$$+$$

Fig.1

T.Hotta and S.Fujimoto

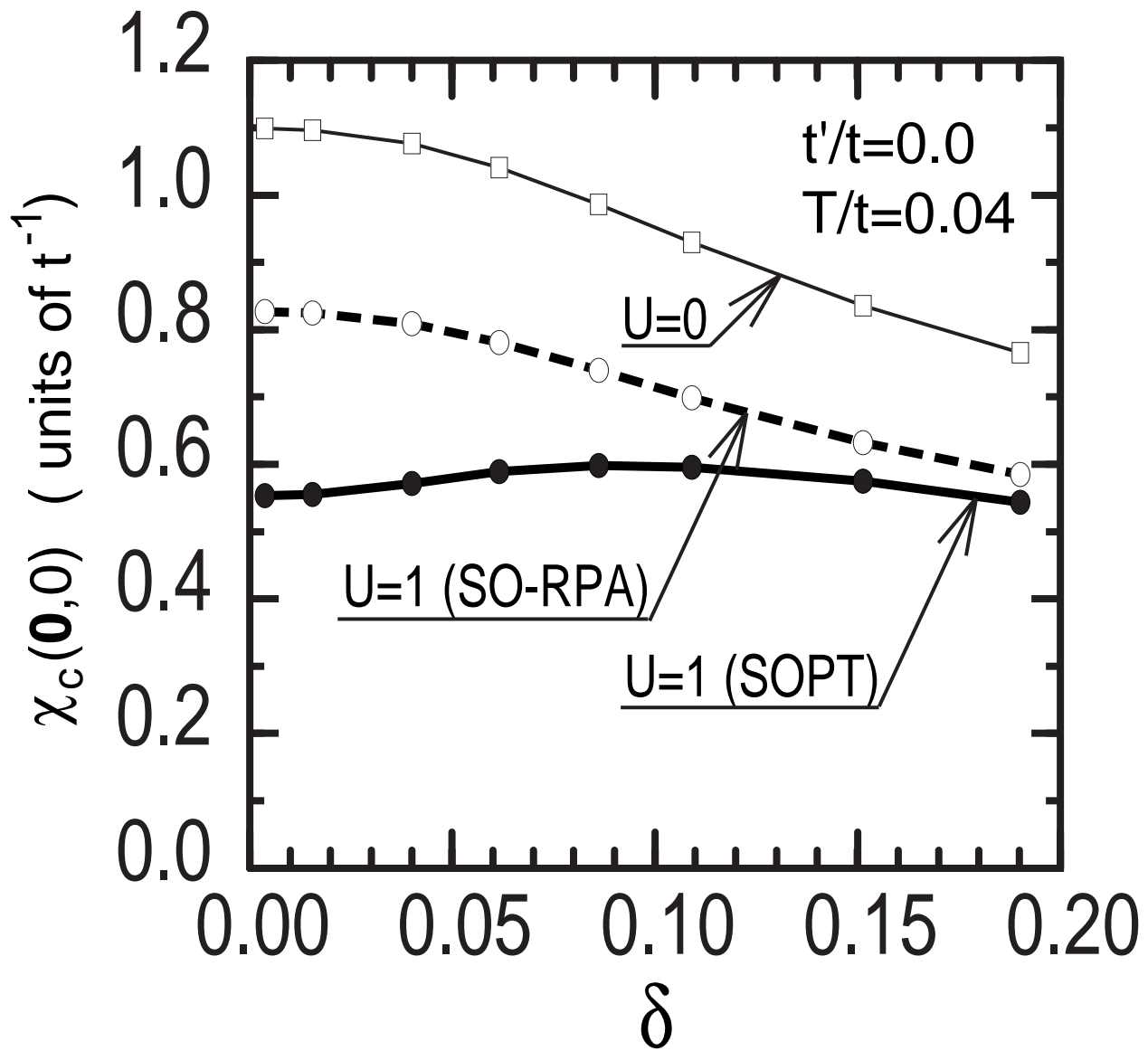


Fig.2

T.Hotta and S.Fujimoto

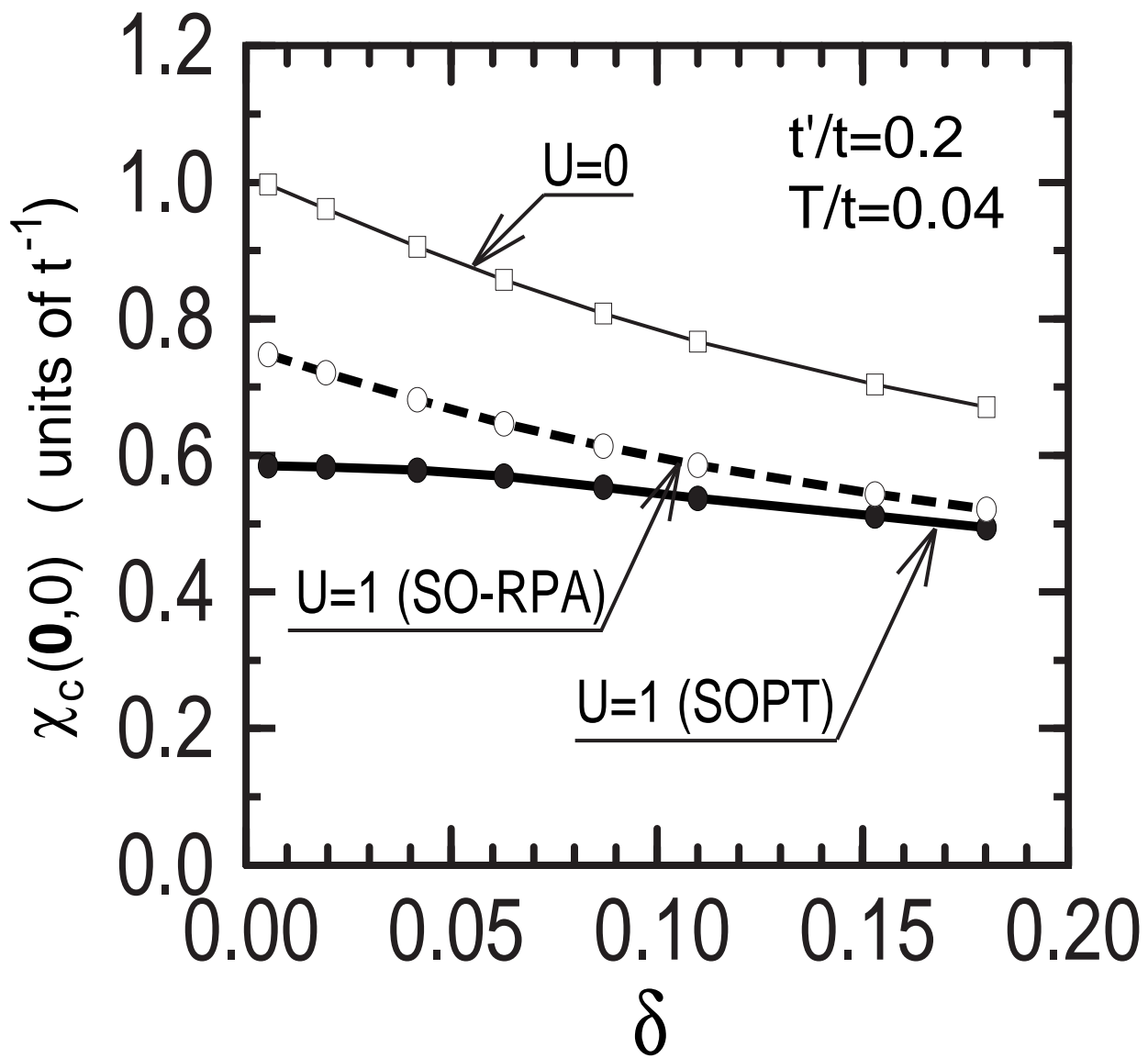


Fig.3 T.Hotta and S.Fujimoto

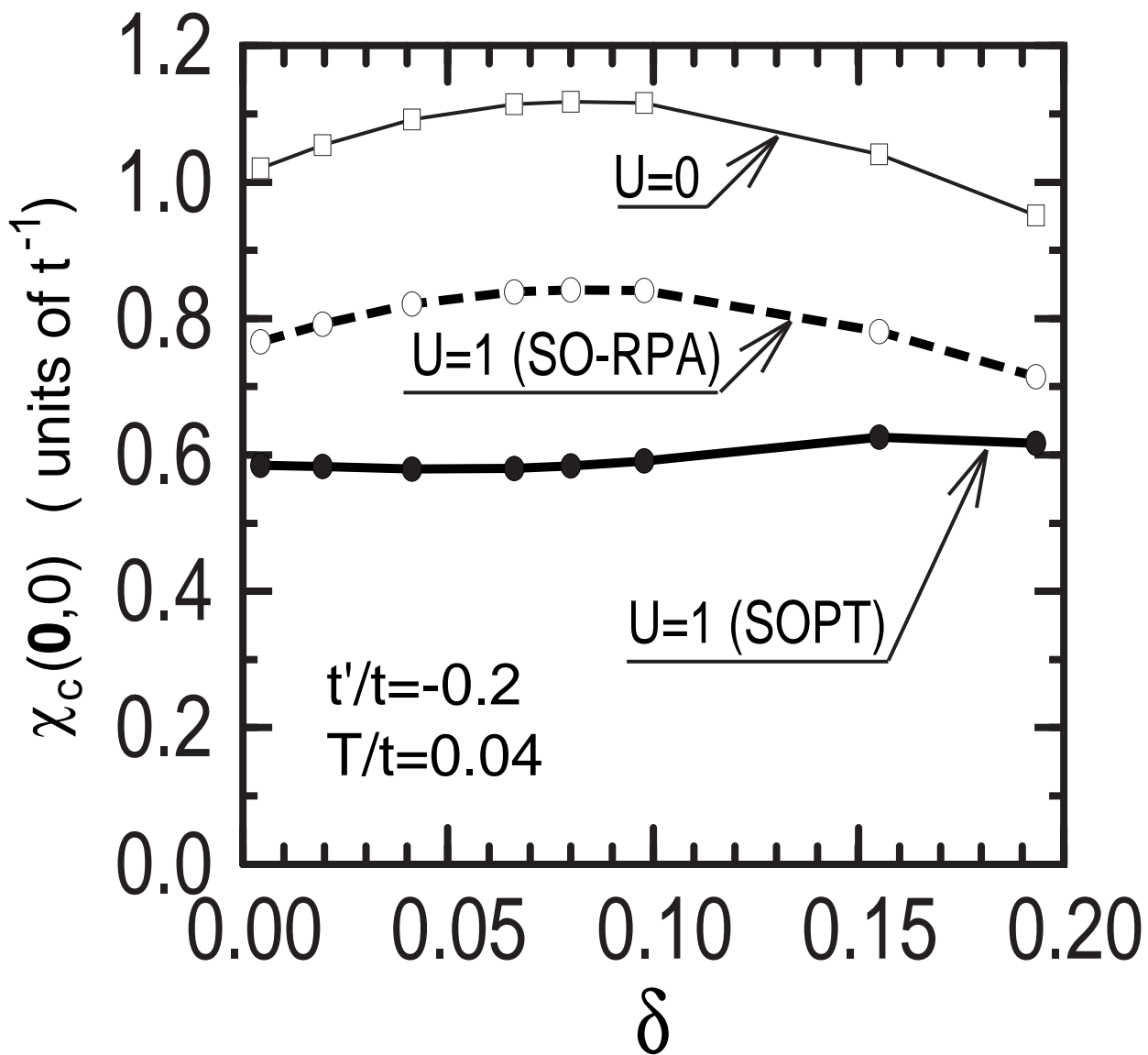


Fig.4

T.Hotta and S.Fujimoto

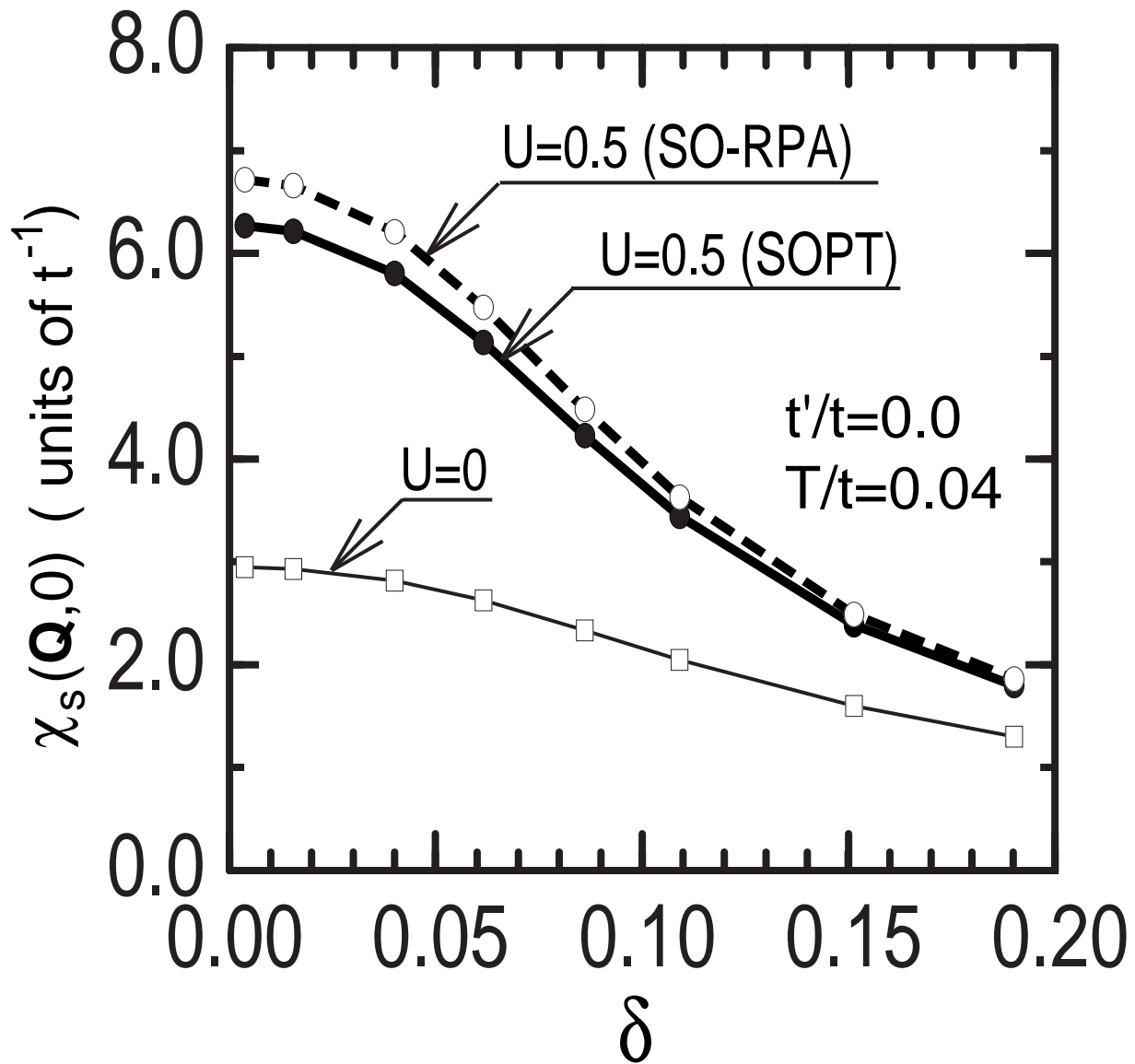


Fig.5

T.Hotta and S.Fujimoto

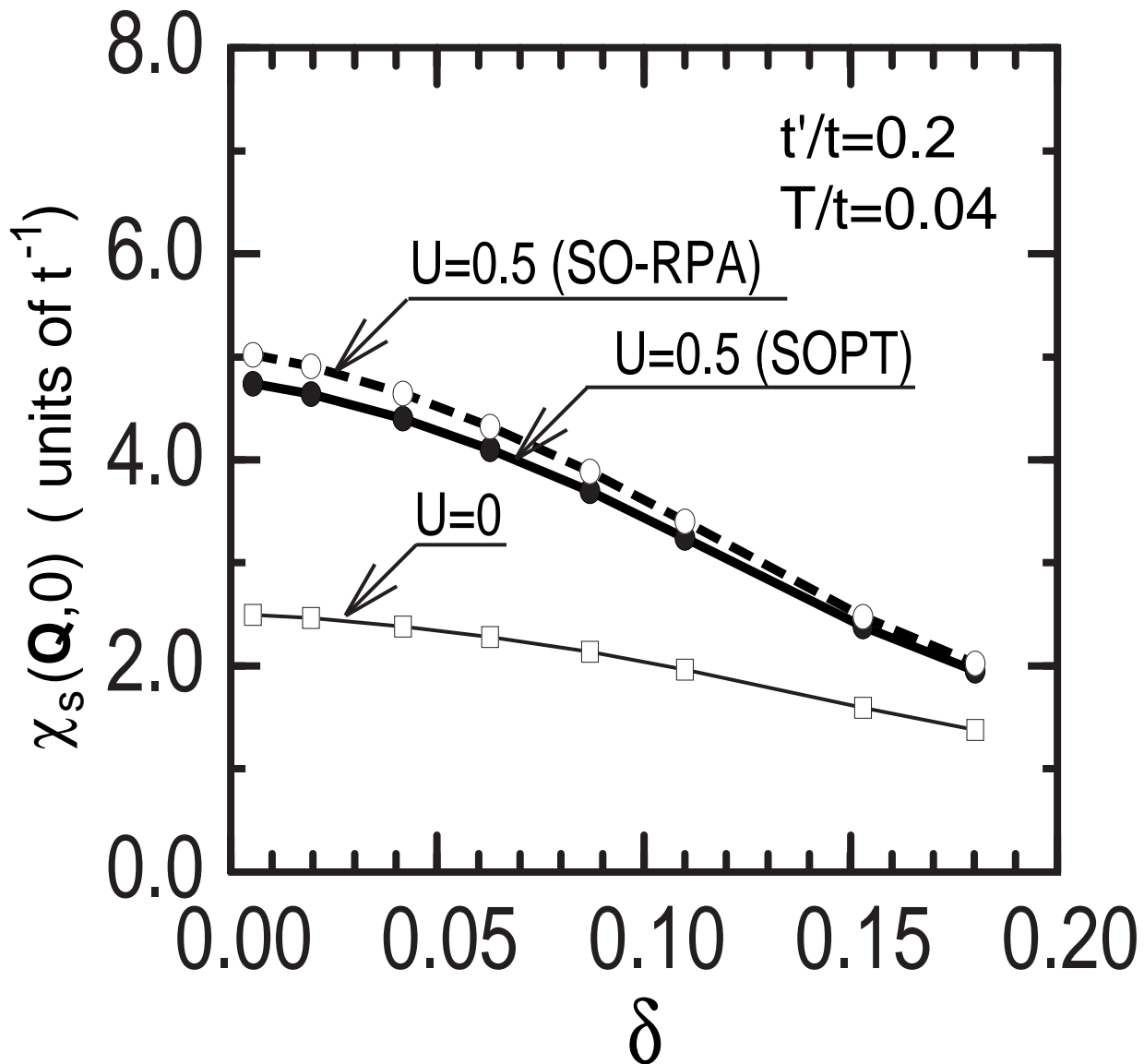


Fig.6

T.Hotta and S.Fujimoto

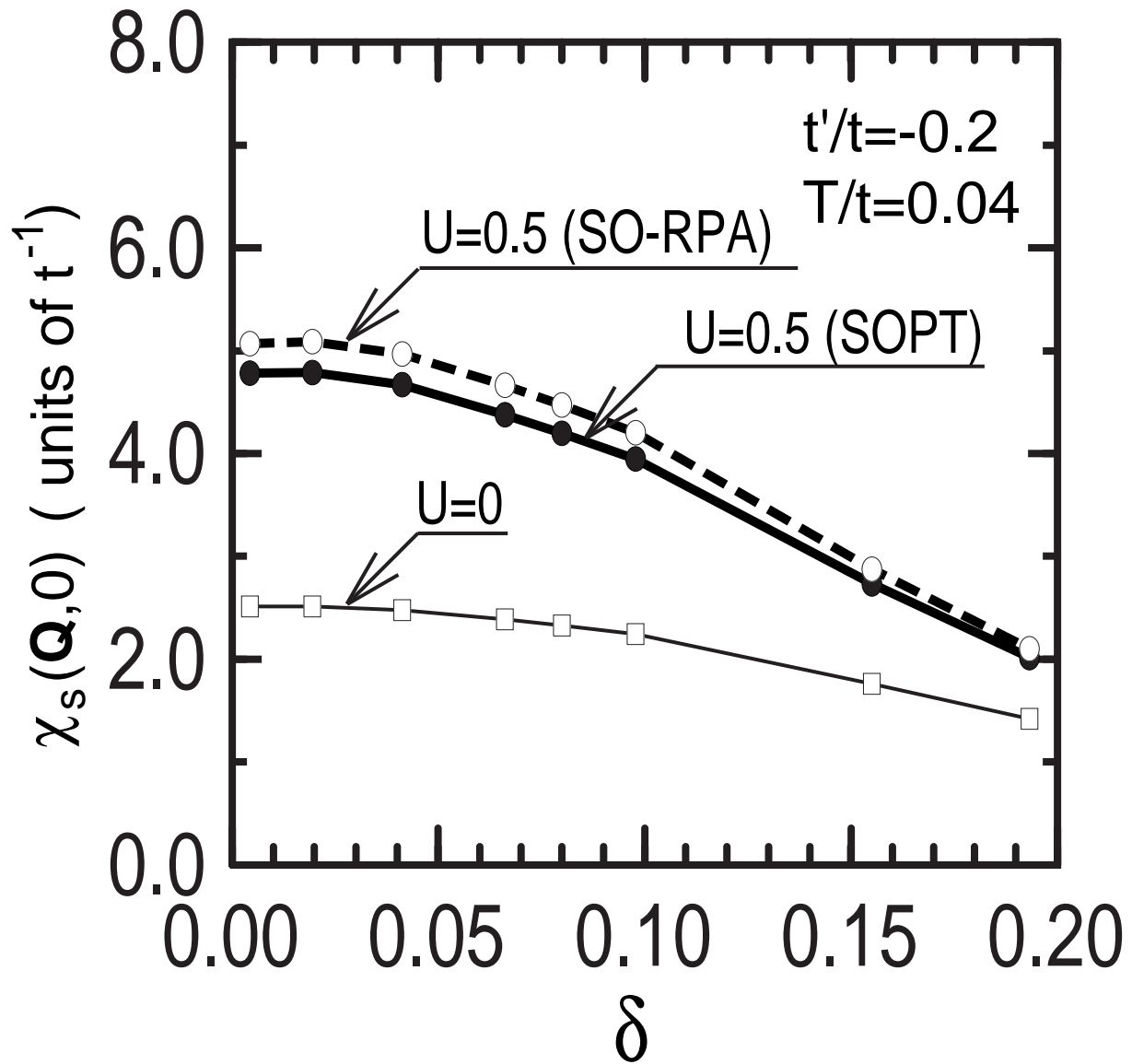


Fig.7

T.Hotta and S.Fujimoto

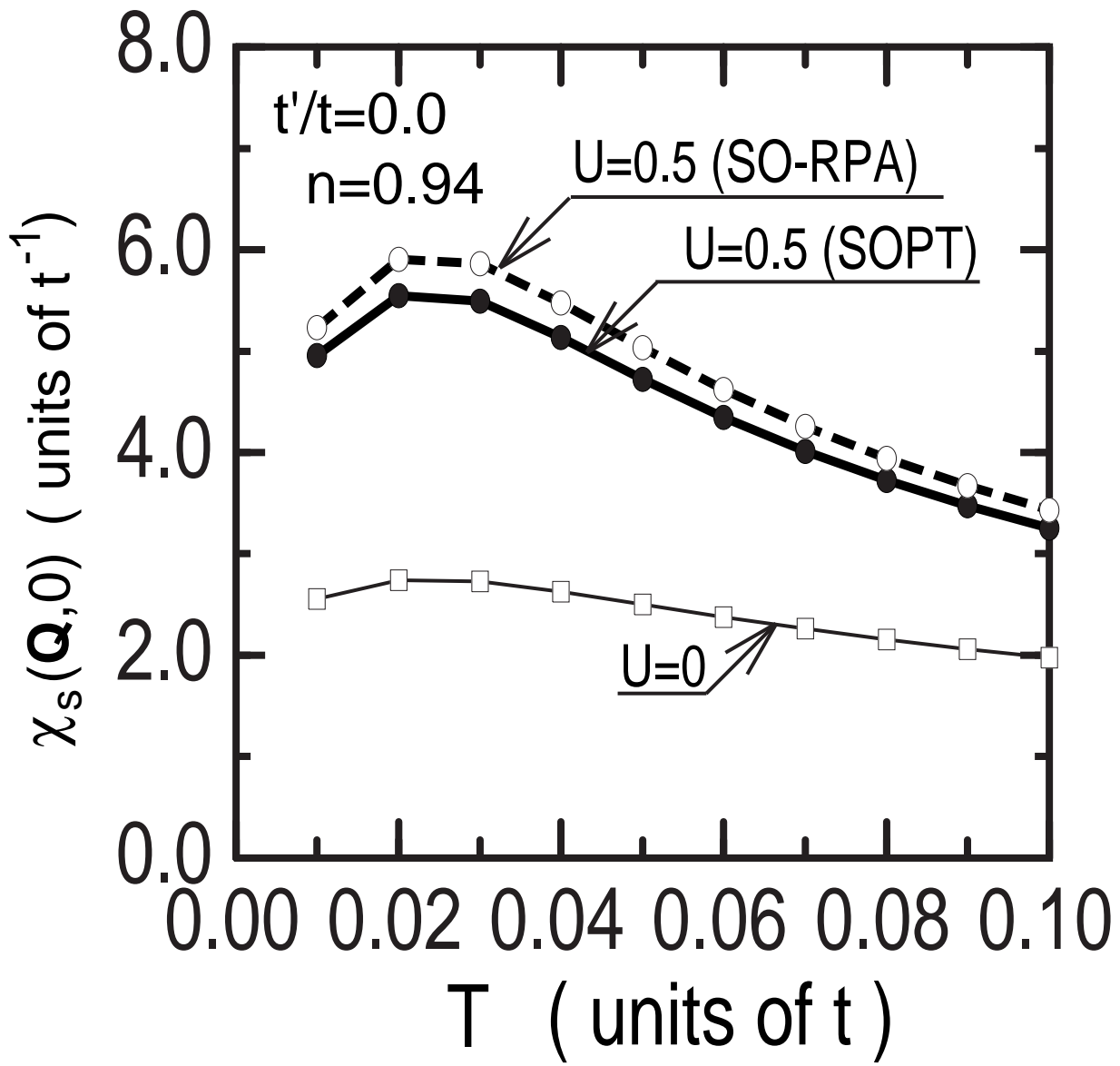


Fig.8

T.Hotta and S.Fujimoto

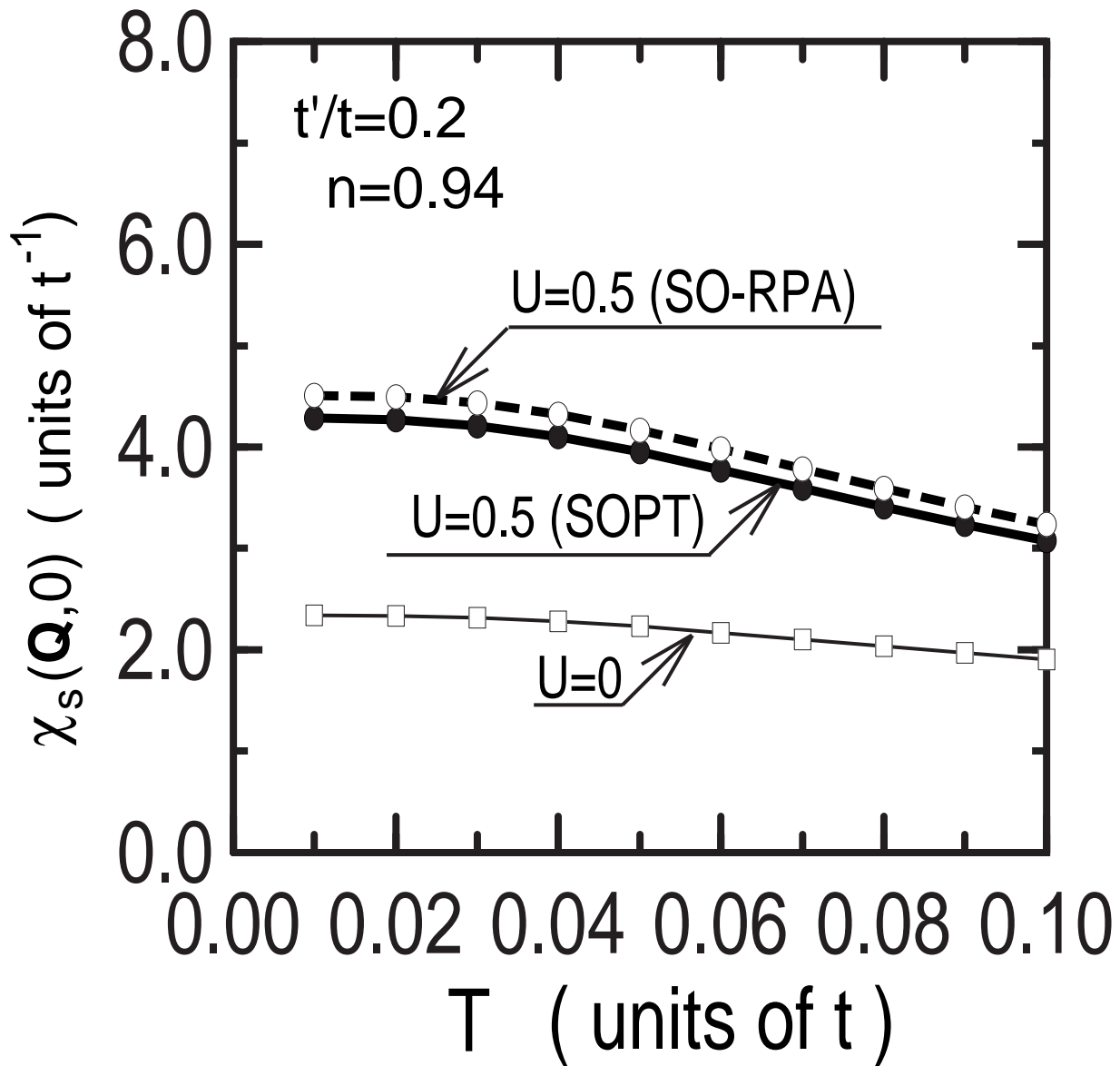


Fig.9

T.Hotta and S.Fujimoto

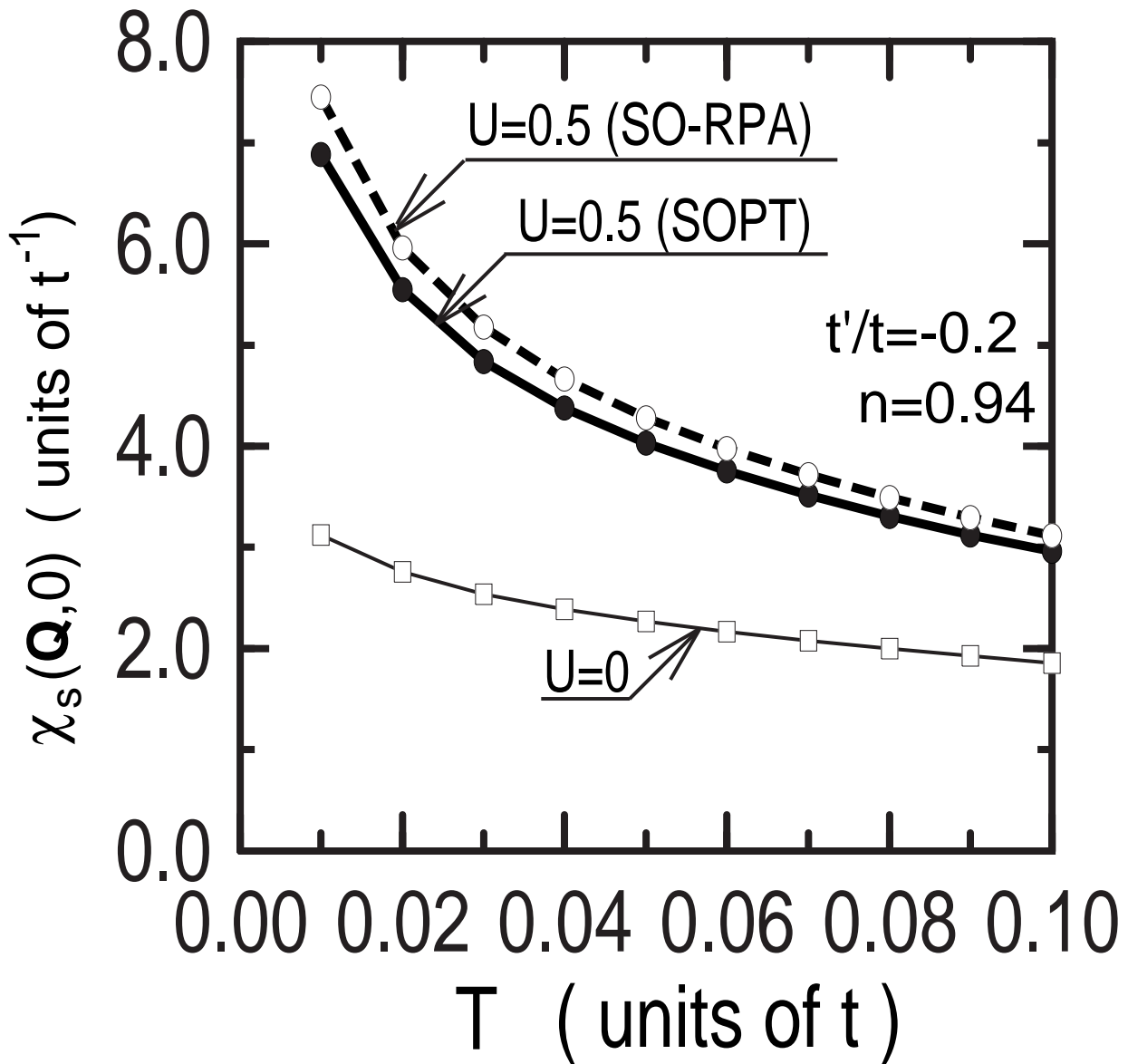


Fig.10

T.Hotta and S.Fujimoto

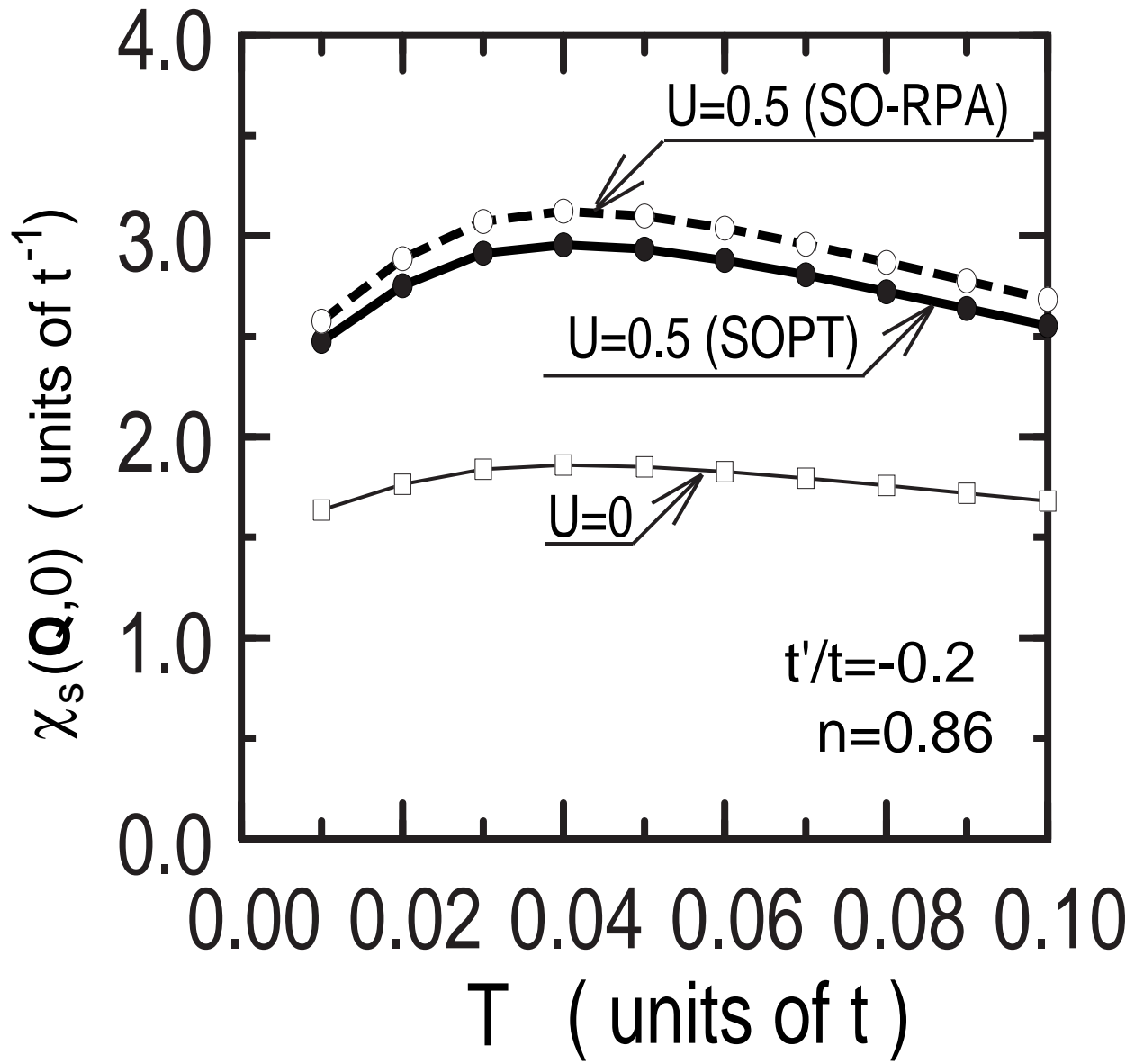


Fig.11

T.Hotta and S.Fujimoto